Embracing LoRa Sensing with Device Mobility

Binbin Xie
University of Massachusetts Amherst
binbinxie@cs.umass.edu

Deepak Ganesan
University of Massachusetts Amherst
dganesan@cs.umass.edu

Jie Xiong
University of Massachusetts Amherst
jxiong@cs.umass.edu

ABSTRACT

Wireless sensing is an emerging technology that can obtain rich context information of human targets in a contact-free manner. Though promising, a missing component of current wireless sensing is sensing under device motions. In this work, we propose to integrate wireless sensing with the mobility of a robot. This is non-trivial because we find that device motions can severely degrade the sensing performance and even completely fail existing wireless sensing systems. In this paper, we propose novel signal processing schemes to address the impact of device motions to enable sensing with device mobility. For the first time, we integrate the robot's mobility with LoRa sensing to enlarge the sensing coverage. Comprehensive experiments demonstrate the effectiveness of the proposed system. We employ two representative sensing applications, i.e., fine-grained respiration monitoring and coarse-grained human walking sensing, to showcase the performance of our system. The proposed system is able to achieve accurate sensing in the presence of device motions, moving wireless sensing one step forward towards truly ubiquitous sensing for real-life adoption.

CCS CONCEPTS

• **Human-centered computing** → *Ubiquitous and mobile computing systems and tools*.

KEYWORDS

LoRa sensing, integration of wireless sensing and device mobility, device motion removal, interference mitigation

ACM Reference Format:
Binbin Xie, Deepak Ganesan, and Jie Xiong. 2022. Embracing LoRa Sensing with Device Mobility. In *The 20th ACM Conference on Embedded Networked Sensor Systems (SenSys '22), November 6–9, 2022, Boston, MA, USA.* ACM, New York, NY, USA, 13 pages. https://doi.org/10.1145/3560905.3568524

1 INTRODUCTION

While wireless signals have been widely used for communication, recent years have witnessed the progress of exploiting pervasive wireless signals for sensing purposes. A large range of applications have been enabled, ranging from coarse-grained activity recognition [31], gait sensing [41], fall detection [20] to fine-grained respiration monitoring [49] and finger tracking [16]. The basic principle behind wireless sensing is that wireless signals vary with target movements. By analyzing the variation of signal reflection from the target, the target's context information can be sensed. Different from traditional sensor-based sensing, wireless sensing is achieved without a need of attaching any sensors to the target in a contact-free manner. The unique characteristics of wireless sensing attracted attentions from both academia and industry. Google's Soli project [4] is a great example of wireless sensing and the mmWave sensing module has been integrated into Google Pixel smartphones. Apple and Samsung have also embedded UWB modules in their latest smartphones [11, 13] for ranging and sensing purposes.

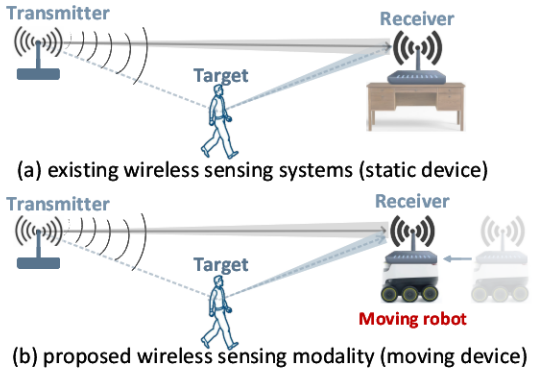

Figure 1: Comparing wireless sensing between using: (a) static device, and (b) moving device.

Although promising, one fundamental problem associated with wireless sensing is that the sensing device is kept static, e.g., deployed on the ground or placed on a table. However, the sensing device can be non-static in quite a lot of real-life scenarios. For example, hospitals are using robots to remotely monitor the vital signs of patients to help reduce the exposure to infectious virus such as COVID-19. In a nursing home, a robot with sensing modules can follow the elderly to continuously sense the target and save life in case of emergency. If the sensing system can only work with static device, the robot needs to stop before it can sense the target movement, which greatly limits its applicability. We believe sensing in the presence of device motions is an important missing piece of wireless sensing.

Among diverse wireless technologies being employed for sensing, LoRa is promising owing to its larger sensing coverage. Due to the nature of relying on reflection signals for sensing, there exists a huge gap between communication range and sensing range. Take WiFi as an example, while one WiFi access point can cover the whole apartment for communication, the state-of-the-art WiFi sensing coverage is only one single room [49]. Recent works have exploited LoRa signals which have a much longer communication range for a larger sensing coverage [43, 46, 50]. However, with blockages such

SenSys '22, November 6–9, 2022, Boston, MA, USA

ACM ISBN 978-1-4503-9886-2/22/11…$15.00
https://doi.org/10.1145/3560905.3568524

as walls and furniture in real-world settings, the achieved sensing coverage is still limited even with LoRa.

In this work, we propose *RobotSen*, which places LoRa device on a moving robot to study the feasibility of wireless sensing in the presence of device motions. With a robot moving the LoRa device, wireless sensing can be performed in a larger area. Wireless sensing also adds a new sensing modality to robot platform which traditionally relies on camera and LiDAR for sensing.

However, we quickly realize making wireless sensing work with a moving device (i.e., the device is placed on a moving robot) is challenging. Almost all existing wireless sensing systems keep their devices static as shown in Figure 1(a) and very little attention has been paid to wireless sensing with a moving device. This is because wireless sensing fundamentally relies on signal variations to sense target movement. When the device is static, signal variations are only induced by target movements. However, if the device is also moving, the signal variations are then induced by both target movements and device motions. It is therefore difficult to separate target movements from device motions to achieve target sensing. The straightforward method to deal with device motions is to obtain the motion information using the sensors equipped with the robot. For example, moving speed can be obtained from an accelerometer. However, sensor readings are too coarse to be used to cancel the motion effect for fine-grained sensing such as respiration monitoring on the scale of a few millimeters.

In this work, we employ the signal propagation theory to understand the effect of device motion on signal variation and address it to achieve target sensing under device motions. Similar to target movement which causes the signal amplitude and phase to change, the device motion causes an extra amount of signal variation. If we can remove the extra amount of signal variation caused by device motion, we can obtain clean target-induced signal variation for sensing. The key idea of our design is to utilize a second antenna to remove the signal variation induced by device motion. The intuition is that during the robot movement process, the second antenna moves to the previous location of the first antenna. When two antennas are at the same location, the reflections from static objects are very similar and therefore we can leverage the signals received at the two antennas at the same location to remove these reflections. On the other hand, the target movements are different and the cancellation process does not eliminate the target movement information. We further remove the remaining effect of device motion leveraging the periodicity of the target-induced signal variation pattern. By placing two antennas along the moving directions of the robot, the two antennas move following the same trajectory during the robot movement process.

Contributions: The main contributions are as follows:

- We combine the sensing capability of LoRa signals with the mobility of robot to support a larger sensing coverage.
- With a deep understanding of the effect of device motion on signal variation, we propose a novel method which utilizes the same moving trajectory of two antennas to eliminate signal variation induced by device motion.
- We evaluate the performance of *RobotSen* using two representative applications, i.e., fine-grained respiration monitoring and coarse-grained walking sensing. While *RobotSen* is implemented on LoRa hardware, the proposed method can also benefit other wireless sensing modalities.

2 PRELIMINARY

In this section, we introduce the LoRa basics, and the principle of LoRa sensing when LoRa device is static. Then we use two examples to show how device motions affect wireless sensing.

2.1 LoRa Basics

LoRa, a low-power wide-area wireless technology designed for connections among IoT devices, can support a communication range on the scale of kilometers in rural areas [22, 26, 27, 42]. Recent works [14, 46, 50] demonstrate that LoRa sensing can also achieve a larger sensing range compared to other wireless technologies such as WiFi [49]. The long range is mainly owing to the Chirp Spread Spectrum (CSS) modulation design which can enable LoRa to detect weak signals even 20 dB below the noise floor [26]. Although the sensing range of LoRa is larger, the sensing coverage is still not enough to cover a large space such as a warehouse.

2.2 LoRa Sensing with Static Device

LoRa signal goes directly from the transmitter to receiver, and also gets reflected from the target and other objects. To analyze how signals vary with target movement, we group the signal paths into two categories, i.e., static path and dynamic path [43, 50]. The static paths are composed of the direct path and reflection paths from static objects, while the dynamic path is the target reflection path. During the target movement process, the path length of dynamic path changes while the length of static path does not change. The amount of path length change is determined by the displacement of target movement. For instance, the chest displacement during respiration is around 5 mm, and the induced path length change is around 1 cm. On the other hand, human walking-induced path length change can be several meters.

2.3 Impact of Device Motion on Sensing

To show how device motion affects sensing, we conduct benchmark experiments with two applications, i.e., fine-grained respiration monitoring and coarse-grained human walking sensing. The chest displacement during respiration is around 5 mm while the device on the robot can move on the scale of meters in a few seconds. As shown in Figure 2(a), when the receiver is static, we can see a clear periodical respiration pattern. However, once the receiver starts moving with a robot at a speed of 0.2 m/s, the respiration-induced phase variation pattern is severely distorted as shown in Figure 2(b). This is because when the receiver is moving, the phase variation induced by device motion is much larger than that induced by chest displacement. Thus, respiration-induced phase variation is buried in the phase variation induced by device motion. When the target walks 1 m away from the static device, the path length would be changed by roughly 2 m, inducing a phase change of $\frac{2m}{33cm} = 6.1$ cycles[1] as shown in Figure 2(c). When the device is moving, the walking pattern is severely distorted as presented in Figure 2(d).

3 SYSTEM DESIGN

Without loss of generality, we consider the case when LoRa transmitter is static and LoRa receiver moves with a robot. We first

[1]The wavelength is around 33 cm for 915 MHz LoRa signals.

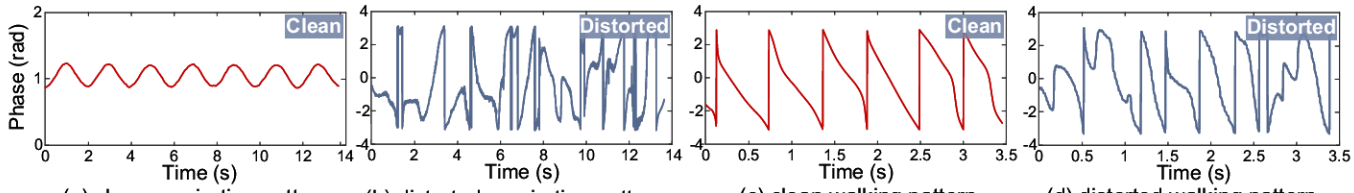

(a) clean respiration pattern when device is static (b) distorted respiration pattern when device is moving (c) clean walking pattern when device is static (d) distorted walking pattern when device is moving

Figure 2: Impact of device mobility on respiration sensing and walking sensing.

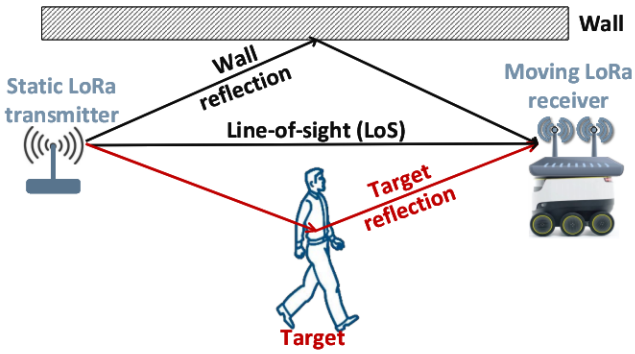

Figure 3: A simple scenario for sensing with a moving receiver.

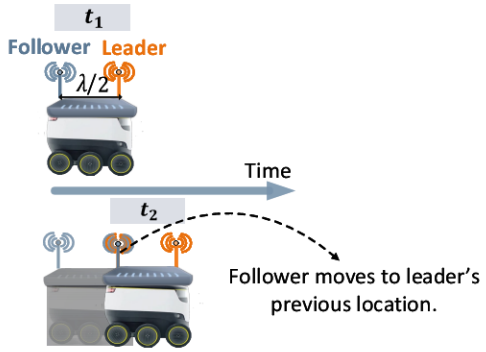

Figure 4: Leader-follower antennas.

theoretically analyze the effect of device motions on received signal, and then present how to address the signal variation induced by device motion. Finally, we show how to deal with the random phase offset due to unsynchronization between the transmitter and receiver.

3.1 Modeling Sensing under Device Motion

To illustrate LoRa sensing under device motions, we employ a simple example as shown in Figure 3. A robot carrying the LoRa receiver moves around while the LoRa transmitter is static. Signals arriving at the LoRa receiver contain not only signal reflected by the moving target, but also line-of-sight (LoS) signal and reflection from static objects such as the wall. Note that when the device is moving, the static paths described in Section 2.2 do not exist any more. All the signal paths are now dynamic. We further group these signal paths into two categories: static-device path and target-device path.

- The static-device path means the signal gets reflected from a static object before arriving at the moving receiver. This signal, represented as H_{sd}, contains only the device motion information.
- The target-device path means the signal gets reflected from the target before arriving at the moving receiver. We define the signal as H_{td} which contains the information of both device motion and target movement.

As both the static-device signal and target-device signal vary over time, the received signal can be written as $R(t) = H_{sd}(t) + H_{td}(t)$. The fundamental rationale behind wireless sensing is that the target movement causes signal variation at the receiver which can be utilized to derive the target information. If the LoRa receiver is static, the target-induced signal variation can be directly employed for sensing. However, a moving device can cause an additional signal variation, interfering target sensing. Therefore, to enable sensing in the presence of device motions, we need to remove the additional signal variation caused by device motions.

3.2 Leader-follower Antennas

To extract clean target-induced signal variation, we first need to remove the *static-device signals* which only involve device motion, and then address the variation caused by device motion on the *target-device signal*. However, this is challenging because the channel bandwidth of LoRa is at most 500 kHz and the number of antennas equipped at the LoRa receiver is also limited. It is therefore difficult to separate signals in either time domain or spatial domain. Moreover, the device motion is on the scale of meters, which can be much larger than the target movement such as respiration (i.e., 5 mm chest displacement), making it challenging to extract clean target signal variation.

Our key idea is to employ a second antenna available at the LoRa receiver as shown in Figure 4 to address the impact of device motion through delicate signal processing. When two antennas are aligned along the moving direction of the robot, the second antenna will arrive at the previous location of the first antenna after a time delay. We call the first antenna *the leader antenna* and the second antenna *the follower antenna* in our design. When two antennas are at the same location, the static-device signals only related to device motion are very similar, therefore, we can cancel them via signal subtraction. However, the target-device signals are different because target movements are different at different timestamps. In this work, we propose to utilize the difference between two target-device signals for sensing. This is based on one interesting observation that the phase variation induced by target movement can be enlarged in the

signal difference. We further propose a method to remove the effect of device motion on the target-device signal to extract clean target-induced phase variation for sensing.

Our assumption is that the leader and follower antennas are aligned with the moving direction of robot. Most robots have a camera or sensor at the front side to detect obstacles during the moving process [3, 7, 10]. Robots move with the front side heading forward. When a robot encounters an obstacle and needs to change the moving direction, it first rotates its front side towards the chosen direction, and then moves forward. By leveraging this property, we can align two antennas with the robot's front side to ensure the two antennas follow the same moving trajectory. We also assume the multipath does not vary much within a short period of time, and the robot moving velocity does not change when we measure the signals at the two antennas.

3.3 Removing Device Motion Induced Signal Variation

In this section, we introduce how to address the effect of device motion to obtain clean target-induced signal phase variation.

3.3.1 Signal subtraction. In this subsection, we utilize signal subtraction to remove the static-device signals which contain only device motion.

At time t_2 in Figure 4, the follower antenna moves to the location where the leader antenna was located at time t_1. The received signal $R_L(t_1)$ at the leader antenna and received signal $R_F(t_2)$ at the follower antenna can be expressed as

$$\begin{cases} R_L(t_1) = H_{sdL}(t_1) + H_{tdL}(t_1) \\ R_F(t_2) = H_{sdF}(t_2) + H_{tdF}(t_2), \end{cases} \tag{1}$$

where $H_{sdL}(t_1)$ and $H_{sdF}(t_2)$ are the static-device signals at the leader antenna and follower antenna respectively. $H_{tdL}(t_1)$ and $H_{tdF}(t_2)$ are the target-device signals. Note that in the two equations above, the static-device signals $H_{sdL}(t_1)$ and $H_{sdF}(t_2)$ are identical due to the same location of the two antennas, while the two target-device signals are different because the target movements are different at time t_1 and t_2.

The arriving time delay between t_2 and t_1 can be denoted as δ. We utilize t and $t+\delta$ to represent t_1 and t_2, respectively. By taking the subtraction operation of two equations in Eq. (1), we obtain the signal difference ΔS_{td} as

$$\Delta S_{td}(t) = R_L(t) - R_F(t+\delta) = H_{tdL}(t) - H_{tdF}(t+\delta). \tag{2}$$

In this equation, the static-device signals (H_{sdL} and H_{sdF}) which only contain the device motion are cancelled out.

Next, we analyze the effect of device motion on the remaining target-device signal. For the target-device signal, both the target and device cause the signal to vary. We can represent the signal as

$$H_{td}(t) = A(t) e^{\frac{j2\pi}{\lambda}(l_{ini} + l_d(t) + l_{tar}(t))}, \tag{3}$$

where $A(t)$ is the amplitude of the target-device signal, l_{ini} is the initial signal path length without device motion and target movement, l_d is the path length change caused by device motion, l_{tar} is the path length change caused by target movement, and λ is the signal wavelength. Eq. (2) can then be written as

$$\Delta S_{td}(t) = A_1 e^{\frac{j2\pi}{\lambda}(l_{ini} + l_{dL} + l_{tar}(t))} - A_2 e^{\frac{j2\pi}{\lambda}(l_{ini} + l_{dF} + l_{tar}(t+\delta))}, \tag{4}$$

where l_{dL} and l_{dF} are the path length changes caused by the motions of leader antenna and follower antenna, respectively. When the two antennas are at the same location, as we also assume the velocity does not change, we can obtain $l_{dL} = l_{dF}$ and denote them as l_d. Then we can obtain the following equation

$$\Delta S_{td}(t) = \underbrace{A_1 e^{\frac{j2\pi}{\lambda}(l_{ini} + l_d(t))}}_{\text{device motion: } H_d} \cdot \underbrace{[e^{\frac{j2\pi}{\lambda} l_{tar}(t)} - \frac{A_2}{A_1} e^{\frac{j2\pi}{\lambda} l_{tar}(t+\delta)}]}_{\text{target movement: } \Delta H_{tar}}. \tag{5}$$

To derive clean signal phase variation only induced by target movement, we first simplify Eq. (5). We denote the first part as H_d which is only related to device motion, and represent the second part which is only related to target movement as ΔH_{tar}. The difference of the received signals at the two antennas (i.e., Eq. (5)) can therefore be simplified as $\Delta S_{td}(t) = H_d(t) \cdot \Delta H_{tar}(t)$. Moreover, the path length change induced by device motion can be represented as $l_d(t) = vt$ where v is the radial component of device (robot) velocity. In a short period of time, v can be assumed as a constant.

Then, the phase variation induced target movement ϕ_{tar} can be calculated by subtracting the phase variation induced by the device motion (ϕ_d) from the total phase variation ($\phi_{\Delta S_{td}}$)

$$\begin{aligned} \phi_{tar}(t) &= \phi_{\Delta S_{td}}(t) - \phi_d(t) \\ &= \phi_{\Delta S_{td}}(t) - \frac{2\pi}{\lambda}(l_{ini} + vt). \end{aligned} \tag{6}$$

3.3.2 Modeling target movement using signal subtraction. Different from previous works which utilize one target reflection signal to model the target movement [31, 50], we leverage ΔH_{tar} which is the difference between two target signals as illustrated in Eq. (5) to characterize the target movement. We take the fine-grained respiration sensing and coarse-grained walking sensing as application examples to show the phase variation of target signal difference ΔH_{tar}.

Fine-grained respiration sensing. The inhalation and exhalation of chest motions cause the path length of the target signal to change. According to previous studies [49, 50], the chest displacement during respiration is around 5 mm, inducing a path length change of around 1 cm. Thus, the target signal in the IQ domain rotates by around $\frac{1cm}{\lambda} \times 360° = 11°$ for 915 MHz LoRa signal (λ = 33 cm) during the process of respiration. As shown in Figure 5(a), the target signal vector rotates periodically between points A and B during the process of respiration. The signal amplitude is the length of the signal vector while the phase is the angle between the signal vector and the I-axis.

To show the difference ΔH_{tar} between two target signals, we plot the two target signal vectors as shown in Figure 5(b), denoted as H_{tar1} and H_{tar2}. As we can see, the difference of two target signal $\Delta H_{tar} = H_{tar1} - H_{tar2}$ is a new vector denoted in red color. Initially, at $Time$ 1, the first target signal vector H_{tar1} is near point A while the second one H_{tar2} is near point B, thus their signal difference vector $H_{tar1} - H_{tar2}$ points towards the right. When H_{tar1} rotates near point B and H_{tar2} rotates near point A (e.g., $Time$ 2), the target signal difference vector points towards the left. The opposite directions

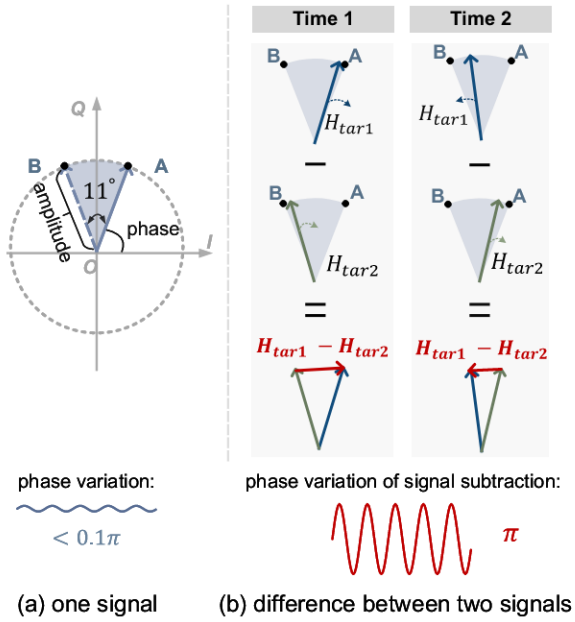

Figure 5: Respiration-induced phase variation of using one signal and using signal difference ΔH_{tar}.

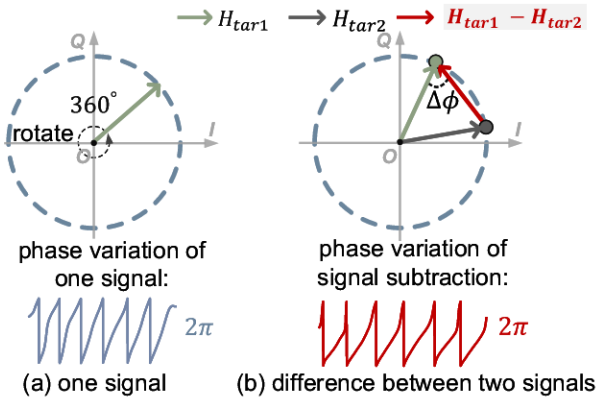

Figure 6: Walking-induced phase variation of using one signal and using signal difference.

of target signal difference vector mean that the respiration-induced phase of ΔH_{tar} varies in the range of $[0, \pi]$ as shown in Figure 5(b). Therefore, even though the chest displacement (i.e., around 5 mm) is small and the induced phase variation at one single target signal is just 11°, the phase variation of the target signal difference (ΔH_{tar}) can be large.

Coarse-grained human walking sensing. Human walking induces the signal path length to vary. Previous works employ one target signal to characterize the target movement. In the IQ vector space as shown in Figure 6(a), the target signal vector rotates during the walking process, and the amount of rotation is determined by the distance the target walks. For example, if the target walks 1 m towards the devices, the path length change is roughly 2 m, corresponding to a phase rotation of $\frac{2\times 1m}{\lambda} = 6.1$ cycles [50]. One cycle of target signal rotation means one wavelength of path length change. Thus, 6.1 cycles of phase rotation induces a total phase variation of 12.2π. As a result, we can calculate the walking distance from the observed amount of phase variation.

Now we introduce the phase variation of target signal difference for walking. In Figure 6(b), the target signal difference ($H_{tar1} - H_{tar2}$ highlighted in red color) rotates with the two target signals H_{tar1} and H_{tar2}. We denote the phase difference between $H_{tar1} - H_{tar2}$ and H_{tar1} as $\Delta\phi$. With H_{tar1} rotating from 0 to 2π, the target signal difference $H_{tar1} - H_{tar2}$ rotates from $\Delta\phi$ to $\Delta\phi + 2\pi$. Therefore, the phase variation of the target signal difference ΔH_{tar} (i.e., $H_{tar1} - H_{tar2}$) is also in the range of $[0, 2\pi]$.

3.3.3 Extracting clean target-induced phase variation. After signal subtraction in Section 3.3.1, we model the impact of remaining device motion in Eq. (6). Now we introduce how to remove the phase variation induced by device motion to extract clean target-induced phase variation.

The target-induced phase variation is distorted by device motion. To extract clean phase variation, we propose a search scheme to remove the phase variation caused by device motion. The key idea is that respiration is a periodic movement and if device motion is removed, clean respiration-induced phase pattern shows a clear periodicity. We can therefore search the optimal v value to maximize the periodicity for device motion removal. As discussed in Eq. (6), the phase variation induced by device motion is equal to $\frac{2\pi}{\lambda}(l_{ini}+vt)$ where l_{ini} and v are unknown. l_{ini} is a constant and does not affect the phase change pattern. Note that v is not the same as the robot velocity V_R. v is the radial component of V_R, and only the radial component contributes to the path length change and accordingly the phase change. The radial component's direction depends on the location of target with respect to the transmitter-receiver pair, which is unknown. Therefore, we can not obtain v directly from the robot's velocity. We search the radial velocity v in the range of $[-V_R, V_R]$ at a step size of 0.01 m/s. In a short time interval, v can be considered as a constant. Based on our empirical studies, we set the time interval as 0.1 s and search the velocity every 0.1 s. During the search process, each velocity v can result in a phase variation of $\frac{2\pi}{\lambda}(vt)$ induced by device motion. We put it into Eq. (6) to remove the phase variation induced by device and derive the target-induced phase variation ϕ_{tar}. To measure the periodicity for respiration-induced signal pattern, we employ the short term Breathing-to-Noise Ratio (BNR) [48] as the metric. We pick the one which has the highest BNR as the clean respiration phase pattern. The corresponding velocity is the optimal radial velocity which can be used to remove the effect of device motion. Clean human walking-induced signal phase pattern also shows clear periodic property and we can search the v to maximize the periodicity which indicates the removal of device motion.

3.4 Dealing with Time-varying Phase Offset

So far we assume that the LoRa transmitter and receiver are synchronized and there is no phase offset in the received signals. In practice, the transmitter and receiver are unsynchronized, leading to random phase readings [18, 50].

Before presenting the proposed method, we first introduce the phase offset in the received LoRa signal. The LoRa transmitter transmits linear chirp signals. Given the initial frequency f_s of chirp, the transmitted chirp signal can be represented as $T(t) = e^{j(2\pi f_s t + \pi k t^2)}$ where k is the chirp slope, i.e., the rate of frequency change [50]. As

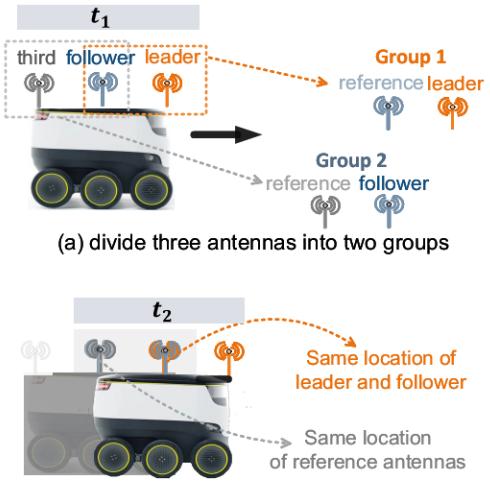

(a) divide three antennas into two groups

(b) Group 2 presents at previous location of Group 1

Figure 7: Adding a third antenna to remove phase offset.

mentioned earlier, the received signal is a superimposition of static-device signals and target-device signal, which can be represented as $R(t) = e^{j(2\pi f_s t + \pi k t^2)}(H_{sd}(t) + H_{td}(t))$.

- **Carrier Frequency Offset (CFO):** Due to hardware imperfection, the oscillator frequency of LoRa transmitter is different from that of LoRa receiver, resulting in carrier frequency offset. The phase offset induced by CFO is denoted as $\theta_c(t)$.
- **Sampling Frequency Offset (SFO):** The received signal is sampled at a different sampling frequency of $F_s^{'}$ instead of the sampling frequency F_s at the transmitter. The phase offset induced by SFO is defined as $\theta_s(t)$.

Therefore, the received signal can be represented as

$$R(t) = \underbrace{e^{j(\theta_c(t)+\theta_s(t)+2\pi f_s t+\pi k t^2)}}_{\text{contain unwanted phase offsets}} \cdot \underbrace{[H_{sd}(t) + H_{td}(t)]}_{\text{contain target \& device motions}}. \quad (7)$$

The straightforward method is to include a third antenna as the reference which has the same oscillator and thus has the same random phase offset as the two antennas (leader and follower). However, this does not work. The reason is presented below. In our design, to address the impact of device motion, we calculate the signal difference between leader and follower antennas when they are at the same location but at different timestamps. If they share the same reference antenna, the reference signals we pick from the reference antenna are different because the reference antenna also moves with the robot and its signals at different timestamps are different. Therefore, although we cancel out the phase offset, the signal difference is corrupted due to different reference signals.

To deal with this problem, we include a third antenna, and divide these three antennas into two groups as shown in Figure 7(a). The first group is the leader and its reference antenna, and the second group is the follower and its reference antenna. Note that the leader's reference antenna is actually the follower, and the follower's reference antenna is the newly added third antenna. The three antennas

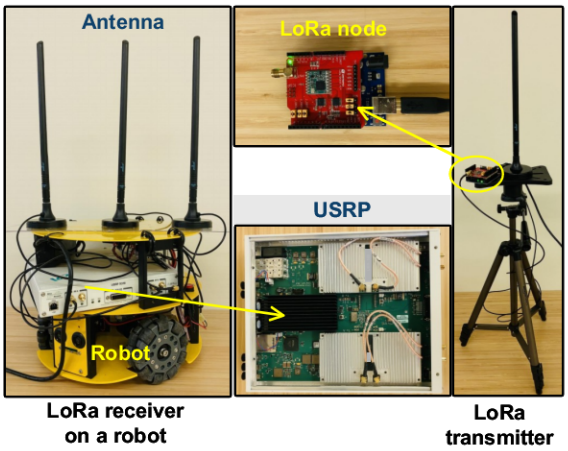

Figure 8: Hardware setup.

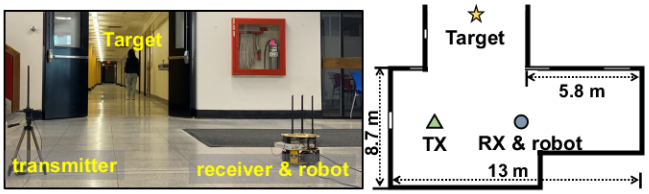

Figure 9: Scenario of benchmark experiment.

share the same oscillator, and thus have the same random phase offset. Our key idea is that the second group will move to the previous location of the first group as shown in Figure 7(b), enabling us to address the impact of device motion and cancel out phase offset at the same time. Specifically, we calculate phase difference between the signals of the leader and follower (serving as the reference) to remove phase offset. We also use the phase difference between the signals of the follower and the third antenna to cancel out phase offset. When the follower moves to the previous location of the leader, their references are exactly at the same location.

4 IMPLEMENTATION

We introduce the implementation of *RobotSen* including the hardware and software. This project is IRB approved by our university.

Hardware. Figure 8 shows the hardware components, including one 3WD Compact Mobile Robot [2], one LoRa gateway as the receiver, and one LoRa node as the transmitter. The prototype of *RobotSen* operates at the carrier frequency of 915 MHz. The mobile robot can be precisely controlled with an Arduino platform. The LoRa receiver with three antennas is placed on the robot while the LoRa transmitter with one antenna is placed on the ground. These antennas are omni-directional [9]. The receiver is built on USRP X310 [12] with a sampling rate of 300 kHz. It collects LoRa signal samples and transfers them via an Ethernet cable to a Thinkpad X1 Extreme laptop for processing. The LoRa transmitter is assembled of a Semtech SX1276 module and an Arduino Uno. The LoRa chirp is configured to have a bandwidth of 125 kHz, a spreading factor of 12, and a duration of 32.8 ms [22, 26].

Software. *RobotSen*'s software implementation contains three key modules: target movement detection, clean target-induced phase

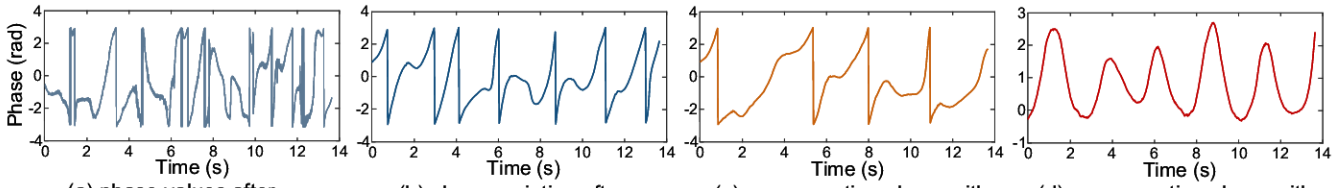

Figure 10: Effect of addressing device motion for respiration monitoring.

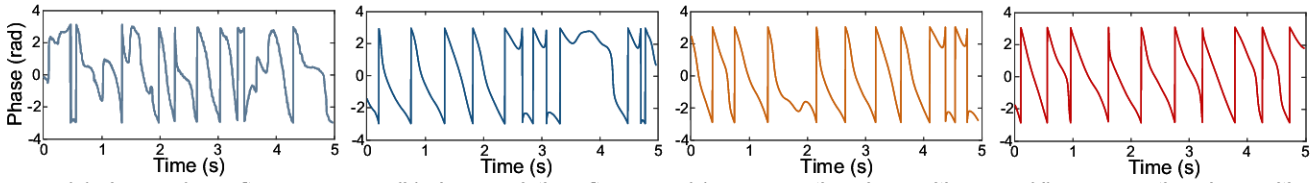

Figure 11: Effect of addressing device motion for walking sensing.

variation extraction, and target sensing (i.e., respiration rate calculation and walking distance estimation). The whole process is implemented using the Labview [8] software and Matlab. Note that the Labview software provides us a compatible interface to integrate compiled Matlab functions with Labview [6].

5 PERFORMANCE EVALUATION

In this section, we first present the benchmark experiments in Section 5.1 to evaluate each component of *RobotSen*. In Section 5.2 and 5.3, we evaluate the performance of *RobotSen* using fine-grained respiration monitoring and coarse-grained walking sensing. We also conduct experiments to evaluate whether *RobotSen* can work in the presence of interference in Section 5.4.

5.1 Benchmark Experiments

We first evaluate the design components of *RobotSen*, i.e., 1) signal subtraction to remove the static-device signals which only contain the device motion (Section 3.3.1); and 2) removal of the phase variation induced by device motion in the target-device signal for clean target-induced phase variation (Section 3.3.3).

Experiment settings. We conduct experiments in a hall and Figure 9 shows the setup of our experiments. The initial distance between the LoRa transmitter and receiver is 3 m, and the LoRa receiver can move with the robot in different directions. The distance between the target and LoRa transceivers is 10 m. For respiration sensing, we calculate the respiration rate using Fast Fourier Transform (FFT), and obtain the ground truth from HEXOSKIN Smart Garments [5]. For walking sensing, we ask the target to walk forward or backward with respect to the LoRa device, and obtain the ground truth using a Laser Distance Meter (Disto E7300) with a millimeter-level accuracy. The default moving velocity of robot is 0.2 m/s, and the default trajectory is a straight line.

For respiration sensing, the signal processing procedure is shown in Figure 10. We collect signals received at the two antennas for around 14 s which contain 5.5 cycles of respiration. Figure 10(a) shows the phase values of the received signal at the leader antenna, where the respiration-induced phase variation is totally buried in that induced by device motion. Figure 10(b) presents the phase variation after signal subtraction, which is cleaner because the static-device signals are removed. Then we remove the phase variation induced by device motion in the target-device signal. Figure 10(c) shows the phase variation by compensating a random radial velocity, which does not present a clear respiration pattern. On the other hand, with the optimal radial velocity compensated, we obtain a clear respiration phase variation pattern in Figure 10(d). The respiration rate of this clean respiration pattern is 23.5 rpm (respirations per minute) which is very close to the ground truth, i.e., 23 rpm.

The signal processing procedure for walking sensing is shown in Figure 11 where the target walks 1.5 m away from the LoRa devices. Similar to that in respiration sensing, the received signals contain multiple static-device signals which change with device motion. The corresponding phase changes randomly as shown in Figure 11(a). After the signal subtraction operation, the phase variation is cleaner as shown in Figure 11(b) which contains both target walking and device motion. Figure 11(c) shows the phase pattern with non-optimal radial velocity of robot compensated. After compensating with the optimal radial velocity, we can remove the phase variation induced by the device motion, and the clean walking-induced phase variation is shown in Figure 11(d). The 9.2 cycles of phase variation indicates a walking distance of $\frac{9.2}{2} \times 33cm = 1.52$ m which is very close to the ground truth (1.5 m).

5.2 Fine-grained Respiration Sensing

In this subsection, we evaluate the performance of *RobotSen* on respiration sensing with a moving device.

5.2.1 Respiration sensing with a moving device. We conduct experiments in three different environments as shown in Figure 12 to evaluate the effectiveness of *RobotSen*. The first scenario is a 17.7 m $\times$ 8.8 m workplace with eight small rooms inside as shown in Figure 12(a). We conduct experiments with the target sitting in different rooms. The second scenario in Figure 12(b) is a large area where the target is sitting in a 9.8 m $\times$ 6.4 m conference room and the receiver

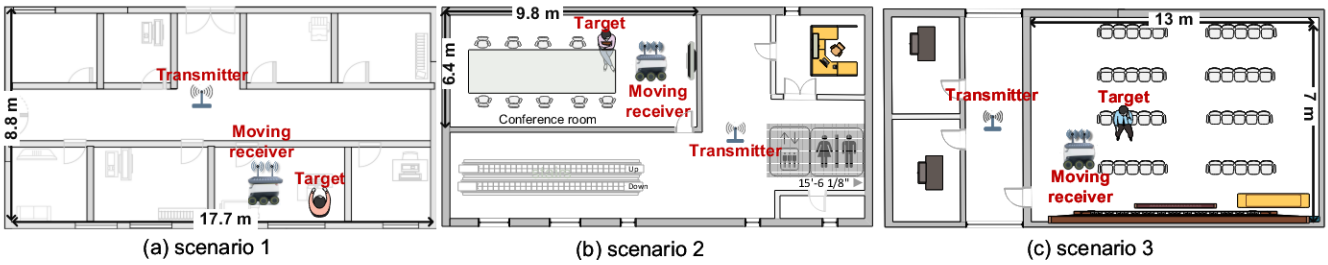

Figure 12: Experiments in three environments.

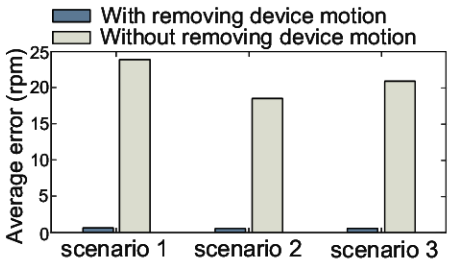

Figure 13: Comparison between with and without removing device method.

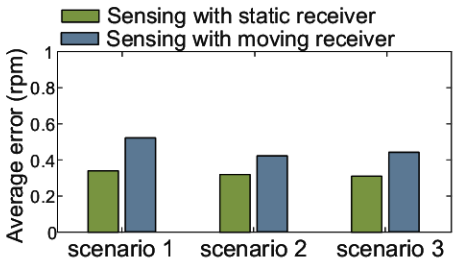

Figure 14: Comparison sensing performance with static and moving devices.

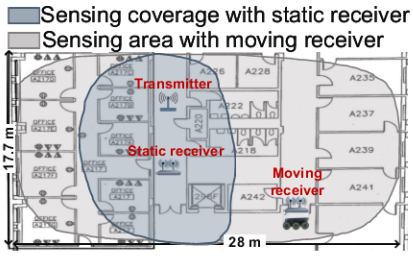

Figure 15: Comparison sensing coverage with static and moving devices

is also moving inside while the transmitter is deployed outside the conference room. The third scenario is a typical classroom with a size of 7 m × 13 m as shown in Figure 12(c). Both the target and moving receiver are located in this classroom while the transmitter is deployed outside the room. In each scenario, we randomly select 20 different target locations to estimate the respiration rate. The default moving velocity of robot is set as 0.2 m/s and we vary the robot velocity in Section 5.2.4 to study the effect.

5.2.2 Effect of removing impact of device motion. To quantify the impact of device motion on target sensing, we compare the sensing performance with and without removing the device motion in these three scenarios. The results are shown in Figure 13. We can observe that the error is significantly reduced in all three scenarios after removing the impact of device motion.

5.2.3 Performance comparison between a static device and a moving device. We also compare the performance between sensing with a moving device and sensing with a static device.

Comparison in terms of accuracy. For sensing with a static device, we conduct experiments 20 times at different target locations and keep the receiver near transmitter. The experiment results for these scenarios are shown in Figure 14. We can see that when the device is static, the average absolute errors are 0.34 rpm, 0.32 rpm, and 0.31 rpm, respectively. When the device is moving, the average errors only slightly increase, i.e., 0.52 rpm, 0.42 rpm, and 0.44 rpm, respectively. The high accuracy in all three environments demonstrates the effectiveness of *RobotSen* in addressing the distortion caused by device motion. Note that *RobotSen* does not intend to improve the sensing accuracy. The novelty of *RobotSen* lies in dealing with impact of device motion and enabling wireless sensing under device motions.

Comparison in terms of sensing coverage in indoor environment. Now we compare the sensing coverage in a typical indoor environment with a large amount of walls and office furniture as shown in Figure 15. For sensing with static device, we deploy the transmitter and receiver in the middle of space to achieve a larger sensing coverage. The distance between static receiver and transmitter is around 8 m. For sensing with a moving device, we do not change the transmitter's location, and let the receiver move around in the corridor. We divide each room or space into 1 m × 1 m grid, and conduct experiments in each grid to check the boundary of sensing coverage. In Figure 15, we can see that with static device, one pair of transceivers can cover around 36% of the whole floor. In contrast, with device mobility, *RobotSen* can cover around 90% of the floor, improving the sensing coverage.

Comparison in terms of dead zone. Dead zone indicates those locations where respiration can not be detected [31] even when the target is inside the sensing coverage. The experiment setup is shown in Figure 16(a). The initial distance between the LoRa transmitter and receiver is 20 m. The target is 2 m away from the transmitter. The locations of transmitter and target do not change, while the receiver moves. For sensing with a moving receiver, we let the LoRa device move with a robot along a predefined trajectory, i.e., move 2.4 m toward and 2.4 m backward twice as shown in Figure 16(a). Figure 16(c) shows the respiration pattern when the device is moving. For sensing with a static device, we place the receiver at 40 different locations along the moving trajectory as shown in Figure 16(b).

We observe very interesting results: there is no dead zone when the LoRa device is moving, but when the device is static, at 17 out of 40 device locations (43%), respiration can not be detected as shown in Figure 16(b). This is because when the LoRa device is static, the received signal is a composite of the static and dynamic signals, and the phase difference between the static and dynamic signals is a key factor affecting the sensing performance [31]. This phase difference is dependent on device location, and the respiration-induced phase variations at some locations are too small to be detected. On the other hand, when LoRa receiver is moving and we apply the proposed method, the static-device signals are canceled out, and the performance is not affected by the static-dynamic signal phase difference.

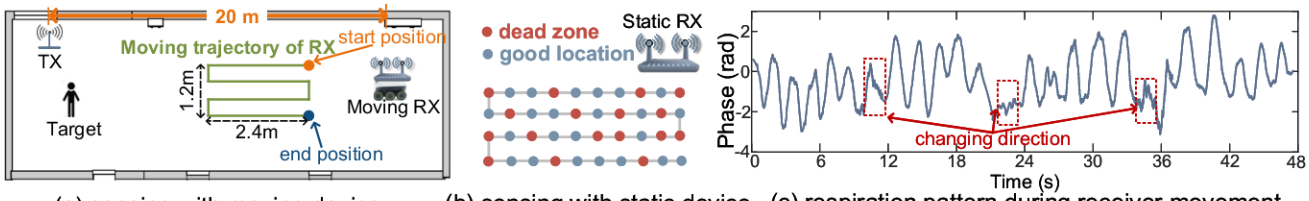

Figure 16: Comparison in terms of dead zone problem.

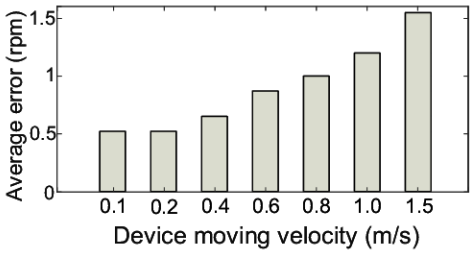

Figure 17: Impact of device moving speed on respiration sensing.

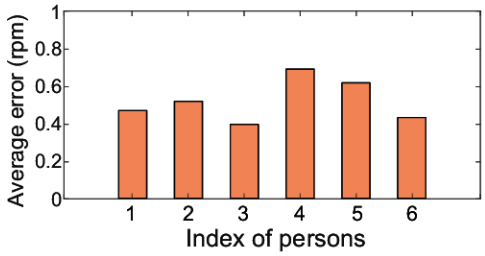

Figure 18: Impact of target diversity on respiration sensing.

The operation of calculating signal difference between two antennas therefore mitigates the dead zone issue in wireless sensing.

5.2.4 Varying key parameters. We now evaluate the impact of device velocity and target diversity on respiration sensing.

Impact of device moving velocity. As shown in Figure 17, the average error of respiration rate estimation increases with the device velocity. When the device moving velocity is smaller than 0.8 m/s, *RobotSen* can achieve an error below 1 rpm which is the accuracy requirement for respiration monitoring. When the device moving velocity is larger than 0.8 m/s, the errors are larger than 1 rpm. This is because higher speed induces larger Doppler shift which can cause errors on the phase readings and accordingly affect the accuracy of respiration monitoring. To make the proposed system works under higher speed, the effect of Doppler shift needs to be addressed.

Impact of target diversity. We also conduct experiments to evaluate the effect of target diversity including gender, weight and height. As shown in Figure 18, the average error of respiration rate estimation varies with different persons. We can observe that person #4 has a higher respiration error compared with other persons. The reason is that the chest displacement of person #4 is smaller than that of other persons.

5.3 Coarse-grained Walking Sensing

Estimating human walking distance without any sensors attached to the target is an interesting topic in contact-free localization and tracking. The default moving velocity of robot is set as 0.2 m/s and we vary the robot velocity in Section 5.3.3 to study the effect.

5.3.1 Wide area walking sensing. With the mobility of robot, the LoRa receiver can move close to the target for sensing. As shown in Figure 19, we conduct experiments on a floor of a building to evaluate the accuracy of walking distance estimation. There are six areas with target locations distributed across the whole floor. For each area, we conduct experiments with the target walking 1 m ~ 10 m, and repeat the experiment for 20 times.

We estimate the walking distance by counting the number of phase rotation cycles [50]. One cycle means the path length change induced by human walking is one wavelength λ and the corresponding walking distance is $\frac{\lambda}{2}$. The cumulative distribution function (CDF) of the walking distance estimation error is shown in Figure 20. The median error is around 6.3 cm when the walking distance is in the range of [1 m, 5 m], and the median error slightly increases to 8.6 cm when the walking distance is in the range of (5 m, 10 m].

5.3.2 Impact of device moving direction. In this experiment, we evaluate the impact of device moving direction with respect to the target. The experiment is conducted in Area 4 of Figure 19. LoRa device moves in six directions with respect to the direct line between the target and device. For each direction, the LoRa device moves with the robot following a straight line. For a same robot velocity, the radial velocities are different in different moving directions. The target stands at 20 different locations in this area and moves towards the LoRa devices for 2 m. The average errors of walking distance estimation are shown in Figure 21, where the errors only vary slightly and are all below 6 cm. The results demonstrate the effectiveness of *RobotSen* when the device moves at different directions.

5.3.3 Impact of device moving velocity. We now configure the LoRa device to move with the robot at varying velocities, i.e., 0.1 m/s, 0.2 m/s, 0.4 m/s, 0.6 m/s, 0.8 m/s, 1 m/s and 1.5 m/s. For each velocity, the LoRa device moves in the same direction. The experiment environment is also Area 4 in Figure 19. Figure 22 shows the errors of walking distance estimation under different robot velocities. As we can see, the estimation error becomes larger with the increase of moving velocity. This is because the phase readings are distorted by Doppler shift and large velocities induce larger Doppler shifts.

5.3.4 Impact of device moving trajectory. We further evaluate the impact of device's moving trajectory. We let the robot move along five different trajectories which are a straight line, a rectangle, a triangle, a "M" shape, and a circle, respectively. The experiment is

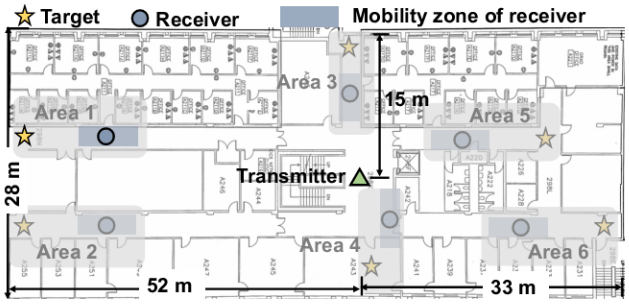

Figure 19: Experiments in a building with one pair of LoRa transceivers.

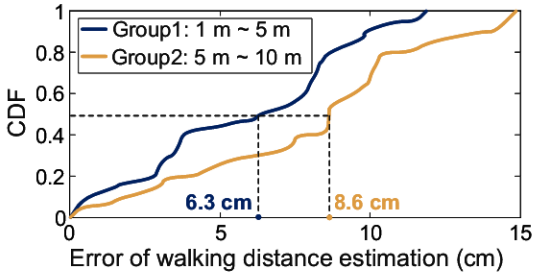

Figure 20: Accuracy of wide-area walking sensing.

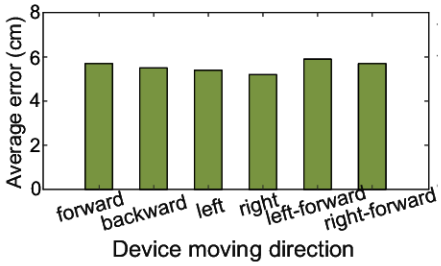

Figure 21: Impact of the device moving direction.

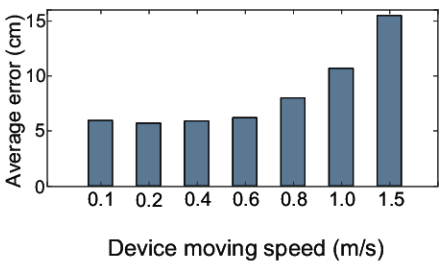

Figure 22: Impact of the device moving velocity.

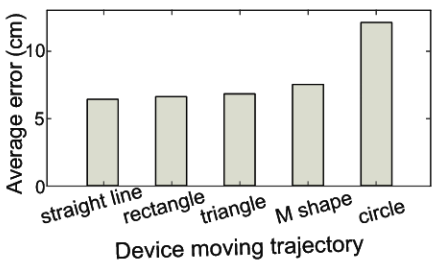

Figure 23: Impact of the device moving trajectory.

also conducted in Area 4 as shown in Figure 19. All these moving trajectories are supported by the robot, and can be configured with the help of the Arduino platform. For each trajectory, the LoRa receiver moves for around 5 s, and we conduct experiments at 20 different target locations. The experiment results are shown in Figure 23 and we can see that the errors are 6.4 cm, 6.6 cm, 6.8 cm, and 7.5 cm for the first four trajectories. We observe a larger error (12.1 cm) for the circle trajectory. This is because in the circle trajectory scenario, the moving direction of the robot keeps changing, making the follower antenna's trajectory not exactly the same as the leader antenna's trajectory, leading to a larger error.

5.4 Dealing with Interference

While larger sensing coverage is preferable in wireless sensing, it also brings one critical issue, i.e., larger interference area. If this issue is not properly addressed, it can greatly degrade the performance of wireless sensing in real-world settings. To address the interference issue, we leverage one interesting observation, i.e., when the transmitter and receiver are separated far away, the effective sensing area is constrained to two small circles surrounding the transmitter and receiver [39], significantly mitigating the interference issue.

5.4.1 Respiration sensing in the presence of interference. We conduct experiments under two different deployments. Deployment I: as shown in Figure 24(a), when we place the transmitter in one room around 20 m away from the conference room with an elevator and a restroom in between, the measured sensing coverage is roughly 5 m surrounding the device, which is highlighted as a blue circle in Figure 24(a). In this scenario, the target is located inside the sensing coverage while four interferers are outside the area. As presented in Figure 24(b), respiration patterns with and without interference for this deployment are quite similar. The large walking-induced interference does not cause issues in this setup. Deployment II: we place the transmitter and receiver in the same conference room with a small transmitter-receiver distance, i.e., 5 m. Under this deployment strategy, the sensing area is large enough to cover both the target and interferers. Even though the interferers are further away from the sensing devices, they can still significantly distort the respiration pattern of the target as shown in Figure 24(c). This experiment demonstrates the effectiveness of separating transmitter and receiver with a large distance to mitigate interference.

5.4.2 Walking sensing in the presence of interference. In this experiment, we evaluate the impact of interference on walking sensing as shown in Figure 25 where the five interferers are randomly located around the target. Among these five interferers, two interferers are walking and the other three are sitting or working. We conduct 20 experiments and ask the target to randomly walk. The distance between the target and the moving device is in the range of [3 m, 5 m]. The experiment results with and without interference are shown in Figure 26. We can observe that with interferers, the error of walking distance estimation only slightly increases from 6.1 cm to 8.8 cm. This result further demonstrate the effectiveness of mitigating interference by placing transmitter and receiver far away (e.g., 28 m in this experiment). The size of sensing coverage can be controlled by changing the transmitter-receiver distance [39].

5.4.3 Sensing with multiple moving receivers. We now conduct experiments to show the feasibility of sensing two targets with two receivers. As shown in Figure 27(a), the two robots carrying two receivers move on the floor of a building. When the transmitter and receiver are separated far away, the effective sensing area is constrained to smaller circles surrounding the transmitter and receiver [39]. Therefore, when two receivers are not close to each other,

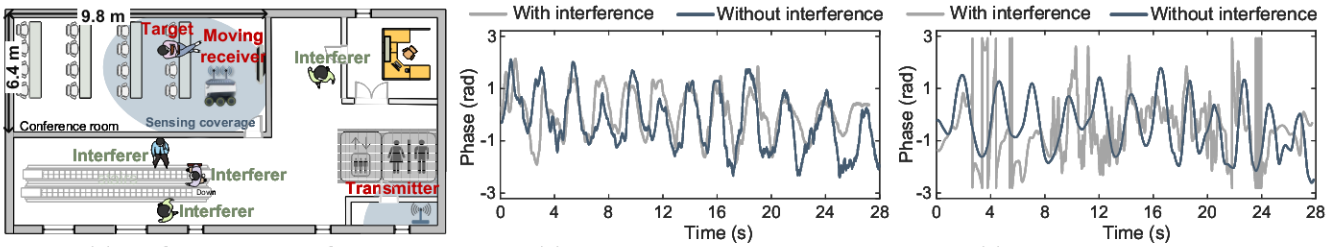

(a) interference scenario for respiration sensing

(b) smaller sensing coverage with interferers outside

(c) larger sensing coverage with interferers inside

Figure 24: Respiration sensing with interference.

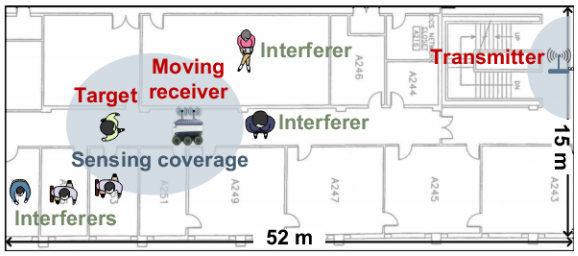

Figure 25: Interference scenario for walking sensing.

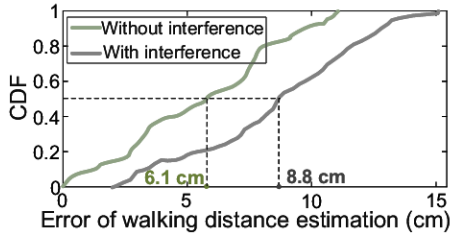

Figure 26: Impact of interference on walking sensing.

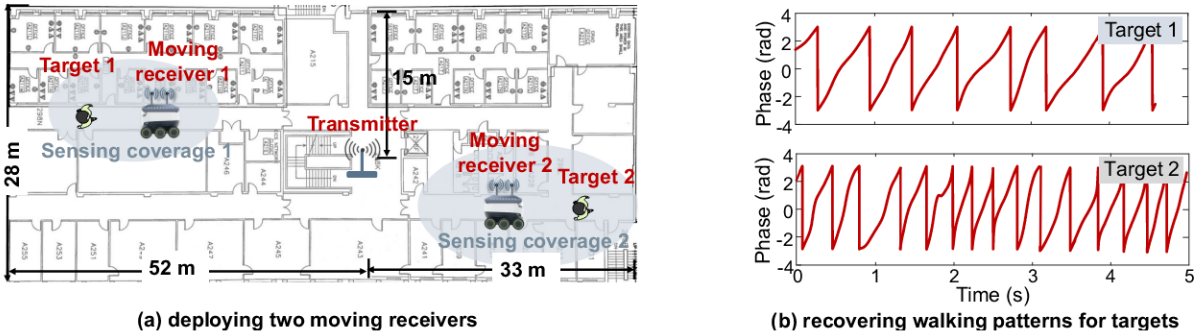

(a) deploying two moving receivers

(b) recovering walking patterns for targets

Figure 27: Sensing with multiple moving receivers.

the sensing coverage does not overlap as presented in Figure 27(a), and thus the two devices can sense without interfering each other. If the two devices are close to each other, interference can occur. In the above experiment, two targets' walking distances are sensed at the same time. The recovered walking-induced patterns are shown in Figure 27(b). For Target 1, the 7.2 cycles of phase variation indicates a walking distance of $\frac{7.2}{2} \times 33cm = 1.19$ m which is very close to the ground truth (1.2 m). For Target 2, the 15.1 cycles of phase variation indicates a walking distance of $\frac{7.2}{2} \times 33cm = 2.49$ m which is also close to the ground truth (2.6 m).

6 DISCUSSION

Sensing random target movements. *RobotSen* can recover periodical respiration and walking patterns, but has difficulties in sensing random target movements such as daily activities under device motions. This is because to remove the impact of device motion, we search the optimal radial velocity by maximizing the periodicity of the clean signal pattern.

Antenna deployment. In our design, we utilize two antennas (leader and follower) to deal with device motion, and also adopt a third antenna to address the random phase offsets due to unsynchronization between LoRa transmitter and receiver. Because the distance between the antennas is set as half wavelength, i.e., 16 cm, this deployment requires a relatively large robot to accommodate the three antennas. To make it work with small robots, we can reduce the distance between adjacent antennas by employing higher-frequency (i.e., 2.4 GHz) LoRa signal with a smaller half wavelength [1]. Another possible option is to leverage the unique chirp properties to remove the phase offsets [22, 42] instead of adopting a third antenna.

Enabling more moving directions. In our design, we configure the line formed by two antennas to be along the moving direction of robot so that the two antennas follow the same trajectory. This works with most robots whose front side is always towards the moving direction. In cases that the antenna line is not the same as the robot moving direction, the performance of *RobotSen* degrades. One potential solution is to change the deployment of antennas (e.g., to a hexagon shape) and utilize the geometric relationship between antennas to create a virtual follower antenna which always follows the same trajectory as the leader antenna.

Multi-target sensing. Multi-target sensing is a well-known challenge in contact-free sensing. When multiple targets exist in the same environment, it is challenging to extract the movement information of each individual target. This is because the reflection signals from multiple targets get mixed together at the receiver. Due to the lack of a large antenna array and a large bandwidth at LoRa receivers [50], it is difficult to separate the mixed signals in either the spatial domain or time domain. One potential solution is to utilize the device mobility to create a virtual antenna array and adopt the method proposed in [47] to fuse information from multiple dimensions (space, time, and frequency) for multi-target sensing.

Deploying sensing device on a drone. In this work, we focus on robot-induced device motions. If we deploy the device on a drone, the device motion would be 3-dimensional. Theoretically, the proposed method in *RobotSen* can also remove the impact of 3D device motion as long as the follower antenna exactly follows the moving trajectory of leader antenna. The challenge is that the drone has more freedom and can move at directions where the leader and follower antennas are not aligned even the drone only moves horizontally. What makes it even more challenging is that the vertical movement of the drone can not be addressed because the antennas are deployed on the same horizontal plane. We believe this is an exciting research direction worth devoting effort to.

7 RELATED WORK

We discuss the most related work in the following domains.

Wireless sensing. Wireless signals have been widely studied for contact-free sensing. Different from sensor and wearable-based methods, wireless sensing does not require the target to carry any device, but relies on analyzing the variation of wireless signals to sense human target. In the last few years, various wireless signals have been employed for contact-free sensing, including Radar [53], WiFi [30, 36, 47], RFID [45], acoustic [23–25, 28], and LTE [19]. While promising in many aspects, one limitation of wireless sensing is the limited sensing coverage. To fully cover a large area, a dense deployment of static devices is required. For instance, only 15% of the area in a typical university building is covered in WiFi sensing range [19]. In this paper, we utilize LoRa signal for contact-free sensing and also explore the feasibility of integrating LoRa sensing with a moving robot to achieve a larger sensing coverage. While mobility requires more space, it saves the cost of deploying many static devices and utilizes a single device efficiently.

LoRa-based sensing. LoRa has been employed for contact-free sensing because of the long sensing range and through-wall capability of LoRa signal. Zhang et al. [50] employ the signal ratio scheme to achieve a sensing range of 25 m for respiration sensing. Zhang et al. [51] also adopt the beamforming technique in LoRa to realize multi-target respiration sensing. Xie et al. [43, 46] further improve the respiration sensing range, and also mitigate the interference issue. None of these works consider device mobility, which we believe is an important step towards ubiquitous wireless sensing. WideSee [15] places LoRa devices on a drone to detect the presence of human targets inside a building. The information obtained in WideSee is still quite coarse. It can not obtain fine-grained respiration information nor the accurate human walking distance because the effect of drone motion is not addressed. In contrast, *RobotSen* moves one step forward to enable fine-grained wireless sensing in the presence of device motions. Palantir [21] attaches LoRa node to a moving bicycle and a backscattered tag to a human target riding the bicycle to sense the target motion. It requires attaching a tag to the target which is not contact-free sensing that *RobotSen* is designed for.

Sensing static objects with robot. UWBMap [17] proposes to combine robot and Ultra Wideband Radar to construct the floor plan. milliMap [29] utilizes a mmWave radar and a lidar co-located on a mobile robot to construct the indoor mapping. LidarPhone [32] captures the sound of a speaker through the lidar sensor on the commodity robot vacuum cleaner. Tagtag [44] employs an RFID antenna moving with a robot to sense the material type of an object with RFID tags attached. However, these systems mainly sense walls, doors, slabs and liquid, which are static. They do not try to sense fine-grained activities such as human respiration which can be easily buried in device motion.

Localizing a moving device. RIM [40] utilizes antennas mounted on the moving receiver to estimate the receiver's moving speed, direction and trajectory. P2PLocate [52] leverages on-body devices to localize a smartwatch. GLAC [35] proposes to localize an RFID tag and employs the tag motion to remove the trajectory ambiguity. In addition, previous RFID-based localization schemes [33, 34, 37] utilize the moving antennas to localize the RFID tags. All these works focus on active localization or sensing.

Wireless communication with device mobility. Prior works [38, 54] have demonstrated the feasibility of utilizing robot/car to realize mobile networks. They utilize the device mobility to enlarge the network coverage. Different from these works, we focus on enabling wireless sensing under device motions, which has different objectives and challenges.

8 CONCLUSION

In this work, we propose *RobotSen*, a contact-free sensing system which can achieve wireless sensing under device motions. We quantify the effect of device motion on sensing and propose a novel leader-follower antenna scheme to address the impact of device motion. Even though the tiny chest displacement during respiration is much smaller than the device motion, the proposed method is able to accurately extract the clean respiration information. We believe the proposed methods can be applied to benefit a large range of wireless sensing applications, moving one important step towards ubiquitous wireless sensing.

ACKNOWLEDGMENTS

This work was partially supported by the NSF under Grant CAREER-2144668, the CCDC Army Research Laboratory (ARL) under Cooperative Agreement W911NF-17-2-0196 (ARL IoBT CRA), and UMass Amherst Institute For Applied Life Sciences (IALS) Equipment Fund. Binbin Xie is supported by Google PhD Fellowship in Mobile Computing. We are grateful to the anonymous shepherd and reviewers whose comments helped bring the paper to its final form.

REFERENCES

[1] 2.4 ghz lora. https://www.semtech.com/products/wireless-rf/lora-connect.
[2] 3wd compact mobile robot. https://www.robotshop.com/en/3wd-compact-omni-directional-arduino-compatible-mobile-robot.html.

[3] Automated guided vehicle. https://www.isa.org/intech-home/2018/july-august/features/automated-guided-vehicles-improve-production.
[4] Google soli. https://atap.google.com/soli/technology/.
[5] Hexoskin smart garments. https://www.hexoskin.com/.
[6] Integrating matlab with labview. https://www.mathworks.com/matlabcentral/fileexchange/61208-labview-matlab-interface-official.
[7] irobot report. https://media.irobot.com/2020-10-20-irobot-reports-third-quarter-2020-financial-results.
[8] Labview. https://www.ettus.com/sdr-software/labview/.
[9] Proxicast antenna. https://www.amazon.com/proxicast-external-compatible-cradlepoint-connectors/dp/b01lxsuu5i.
[10] Robot car. https://www.youtube.com/watch?v=6jljjvsvev8.
[11] Ultra wideband in apple. https://support.apple.com/en-us/ht212274.
[12] Usrp x310. https://www.ettus.com/all-products/x310-kit/.
[13] Uwb in samsung. https://www.sammobile.com/news/uwb-explained-galaxy-s21-plus-s21-ultra.
[14] Z. Chang, F. Zhang, J. Xiong, J. Ma, B. Jin, and D. Zhang. Sensor-free soil moisture sensing using lora signals. *ACM on Interactive, Mobile, Wearable and Ubiquitous Technologies (IMWUT)*, 6(2):1–27, 2022.
[15] L. Chen, J. Xiong, X. Chen, S. I. Lee, K. Chen, D. Han, D. Fang, Z. Tang, and Z. Wang. Widesee: towards wide-area contactless wireless sensing. In *17th Conference on Embedded Networked Sensor Systems (SenSys)*, pages 258–270. ACM, 2019.
[16] M. Chen, P. Yang, J. Xiong, M. Zhang, Y. Lee, C. Xiang, and C. Tian. Your table can be an input panel: Acoustic-based device-free interaction recognition. *ACM on Interactive, Mobile, Wearable and Ubiquitous Technologies (IMWUT)*, 3(1):1–21, 2019.
[17] W. Chen, F. Zhang, T. Gu, K. Zhou, Z. Huo, and D. Zhang. Constructing floor plan through smoke using ultra wideband radar. *ACM on Interactive, Mobile, Wearable and Ubiquitous Technologies (IMWUT)*, 5(4):1–29, 2021.
[18] X. Chen, D. Ganesan, J. Gummeson, and M. Rostami. Cocoon: A conductive substrate-based coupled oscillator network for wireless communication. In *19th ACM Conference on Embedded Networked Sensor Systems (SenSys)*, pages 84–96. ACM, 2021.
[19] Y. Feng, Y. Xie, D. Ganesan, and J. Xiong. Lte-based pervasive sensing across indoor and outdoor. In *19th ACM Conference on Embedded Networked Sensor Systems (SenSys)*, pages 138–151. ACM, 2021.
[20] Y. Hu, F. Zhang, C. Wu, B. Wang, and K. R. Liu. Defall: Environment-independent passive fall detection using wifi. *IEEE Internet of Things Journal (IoTJ)*, 2021.
[21] H. Jiang, J. Zhang, X. Guo, and Y. He. Sense me on the ride: Accurate mobile sensing over a lora backscatter channel. In *19th ACM Conference on Embedded Networked Sensor Systems (SenSys)*, pages 125–137. ACM, 2021.
[22] C. Li, H. Guo, S. Tong, X. Zeng, Z. Cao, M. Zhang, Q. Yan, L. Xiao, J. Wang, and Y. Liu. Nelora: Towards ultra-low snr lora communication with neural-enhanced demodulation. In *19th Conference on Embedded Networked Sensor Systems (SenSys)*, pages 56–68. ACM, 2021.
[23] D. Li, S. Cao, S. I. Lee, and J. Xiong. Experience: practical problems for acoustic sensing. In *28th Annual International Conference on Mobile Computing and Networking (MobiCom)*, pages 381–390. ACM, 2022.
[24] D. Li, J. Liu, S. I. Lee, and J. Xiong. Fm-track: pushing the limits of contactless multi-target tracking using acoustic signals. In *18th Conference on Embedded Networked Sensor Systems (SenSys)*, pages 150–163. ACM, 2020.
[25] D. Li, J. Liu, S. I. Lee, and J. Xiong. Lasense: Pushing the limits of fine-grained activity sensing using acoustic signals. *ACM on Interactive, Mobile, Wearable and Ubiquitous Technologies (IMWUT)*, 6(1):1–27, 2022.
[26] J. C. Liando, A. Gamage, A. W. Tengourtius, and M. Li. Known and unknown facts of lora: Experiences from a large-scale measurement study. *ACM Transactions on Sensor Networks*, 15(2):1–35, 2019.
[27] J. Liu, J. Gao, S. Jha, and W. Hu. Seirios: leveraging multiple channels for lorawan indoor and outdoor localization. In *27th Annual International Conference on Mobile Computing and Networking (MobiCom)*, pages 656–669. ACM, 2021.
[28] J. Liu, D. Li, L. Wang, and J. Xiong. Blinklistener: " listen" to your eye blink using your smartphone. *ACM on Interactive, Mobile, Wearable and Ubiquitous Technologies (IMWUT)*, 5(2):1–27, 2021.
[29] C. X. Lu, S. Rosa, P. Zhao, B. Wang, C. Chen, J. A. Stankovic, N. Trigoni, and A. Markham. See through smoke: robust indoor mapping with low-cost mmwave radar. In *International Conference on Mobile Systems, Applications, and Services (MobiSys)*, pages 14–27. ACM, 2020.
[30] J. Ni, F. Zhang, J. Xiong, Q. Huang, Z. Chang, J. Ma, B. Xie, P. Wang, G. Bian, X. Li, et al. Experience: pushing indoor localization from laboratory to the wild. In *28th Annual International Conference on Mobile Computing and Networking (MobiCom)*, pages 147–157. ACM, 2022.
[31] K. Niu, F. Zhang, J. Xiong, X. Li, E. Yi, and D. Zhang. Boosting fine-grained activity sensing by embracing wireless multipath effects. In *ACM International Conference on emerging Networking EXperiments and Technologies (CONEXT)*, pages 139–151. ACM, 2018.
[32] S. Sami, Y. Dai, S. R. X. Tan, N. Roy, and J. Han. Spying with your robot vacuum cleaner: eavesdropping via lidar sensors. In *18th ACM Conference on Embedded Networked Sensor Systems (SenSys)*, pages 354–367. ACM, 2020.
[33] L. Shangguan and K. Jamieson. The design and implementation of a mobile rfid tag sorting robot. In *14th International Conference on Mobile Systems, Applications, and Services (MobiSys)*.
[34] L. Shangguan, Z. Yang, A. X. Liu, Z. Zhou, and Y. Liu. Relative localization of rfid tags using spatial-temporal phase profiling. In *SENIX Symposium on Networked Systems Design and Implementation (NSDI)*, pages 251–263. USENIX, 2015.
[35] H. Wang, S. Chen, and W. Gong. Mobility improves accuracy: Precise robot manipulation with cots rfid systems. In *International Conference on Pervasive Computing and Communications (PerCom)*, pages 1–10. IEEE, 2021.
[36] J. Wang, H. Jiang, J. Xiong, K. Jamieson, X. Chen, D. Fang, and B. Xie. Lifs: low human-effort, device-free localization with fine-grained subcarrier information. In *22nd Annual International Conference on Mobile Computing and Networking (MobiCom)*, pages 243–256. ACM, 2016.
[37] J. Wang and D. Katabi. Dude, where's my card? rfid positioning that works with multipath and non-line of sight. In *ACM Special Interest Group on Data Communication (SIGCOMM)*, pages 51–62. ACM, 2013.
[38] S. Wang, J. Huang, and X. Zhang. Demystifying millimeter-wave v2x: Towards robust and efficient directional connectivity under high mobility. In *26th Annual International Conference on Mobile Computing and Networking (MobiCom)*, pages 1–14. ACM, 2020.
[39] X. Wang, K. Niu, J. Xiong, B. Qian, Z. Yao, T. Lou, and D. Zhang. Placement matters: Understanding the effects of device placement for wifi sensing. *ACM on Interactive, Mobile, Wearable and Ubiquitous Technologies (IMWUT)*, 6(1):1–25, 2022.
[40] C. Wu, F. Zhang, Y. Fan, and K. R. Liu. Rf-based inertial measurement. In *ACM Special Interest Group on Data Communication (SIGCOMM)*, pages 117–129. 2019.
[41] C. Wu, F. Zhang, Y. Hu, and K. R. Liu. Gaitway: Monitoring and recognizing gait speed through the walls. *IEEE Transactions on Mobile Computing (TMC)*, 20(6):2186–2199, 2020.
[42] X. Xia, N. Hou, Y. Zheng, and T. Gu. Pcube: scaling lora concurrent transmissions with reception diversities. In *27th Annual International Conference on Mobile Computing and Networking (MobiCom)*, pages 670–683. ACM, 2021.
[43] B. Xie and J. Xiong. Combating interference for long range lora sensing. In *18th ACM Conference on Embedded Networked Sensor Systems (SenSys)*, pages 69–81. ACM, 2020.
[44] B. Xie, J. Xiong, X. Chen, E. Chai, L. Li, Z. Tang, and D. Fang. Tagtag: material sensing with commodity rfid. In *17th Conference on Embedded Networked Sensor Systems (SenSys)*, pages 338–350. ACM, 2019.
[45] B. Xie, J. Xiong, X. Chen, and D. Fang. Exploring commodity rfid for contactless sub-millimeter vibration sensing. In *18th Annual International Conference on Embedded Networked Sensor Systems (SenSys)*, pages 15–27. ACM, 2020.
[46] B. Xie, Y. Yin, and J. Xiong. Pushing the limits of long range wireless sensing with lora. *Proceedings of the ACM on Interactive, Mobile, Wearable and Ubiquitous Technologies*, 5(3):1–21, 2021.
[47] Y. Xie, J. Xiong, M. Li, and K. Jamieson. md-track: Leveraging multi-dimensionality for passive indoor wi-fi tracking. In *25th Annual International Conference on Mobile Computing and Networking (MobiCom)*, pages 1–16. ACM, 2019.
[48] S. Yue, H. He, H. Wang, H. Rahul, and D. Katabi. Extracting multi-person respiration from entangled rf signals. *ACM on Interactive, Mobile, Wearable and Ubiquitous Technologies (IMWUT)*, 2(2):1–22, 2018.
[49] Y. Zeng, D. Wu, J. Xiong, E. Yi, R. Gao, and D. Zhang. Farsense: Pushing the range limit of wifi-based respiration sensing with csi ratio of two antennas. *ACM on Interactive, Mobile, Wearable and Ubiquitous Technologies (IMWUT)*, 3(3):1–26, 2019.
[50] F. Zhang, Z. Chang, K. Niu, J. Xiong, B. Jin, Q. Lv, and D. Zhang. Exploring lora for long-range through-wall sensing. *ACM on Interactive, Mobile, Wearable and Ubiquitous Technologies (IMWUT)*, 4(2):1–27, 2020.
[51] F. Zhang, Z. Chang, J. Xiong, R. Zheng, J. Ma, K. Niu, B. Jin, and D. Zhang. Unlocking the beamforming potential of lora for long-range multi-target respiration sensing. *ACM on Interactive, Mobile, Wearable and Ubiquitous Technologies (IMWUT)*, 5(2):1–25, 2021.
[52] X. Zhang, W. Wang, X. Xiao, H. Yang, X. Zhang, and T. Jiang. Peer-to-peer localization for single-antenna devices. *ACM on Interactive, Mobile, Wearable and Ubiquitous Technologies (IMWUT)*, 4(3):1–25, 2020.
[53] M. Zhao, S. Yue, D. Katabi, T. S. Jaakkola, and M. T. Bianchi. Learning sleep stages from radio signals: A conditional adversarial architecture. In *International Conference on Machine Learning (ICML)*, pages 4100–4109, 2017.
[54] A. Zhou, S. Xu, S. Wang, J. Huang, S. Yang, T. Wei, X. Zhang, and H. Ma. Robot navigation in radio beam space: Leveraging robotic intelligence for seamless mmwave network coverage. In *International Symposium on Mobile Ad Hoc Networking and Computing (Mobihoc)*, pages 161–170. ACM, 2019.